Mon. Not. R. Astron. Soc. **000**, 000–000 (0000) Printed 13 June 2002 (MN LATEX style file v2.2)

A *Chandra* observation of the X-ray environment and jet of 3C 31

M.J. Hardcastle[1], D.M. Worrall[1], M. Birkinshaw[1], R.A. Laing[2,3] and A.H. Bridle[4]
[1] *Department of Physics, University of Bristol, Tyndall Avenue, Bristol BS8 1TL*
[2] *Space Science and Technology Department, CLRC, Rutherford Appleton Laboratory, Chilton, Didcot, Oxfordshire OX11 0QX*
[3] *University of Oxford, Department of Astrophysics, Nuclear and Astrophysics Laboratory, Keble Road, Oxford OX1 3RH*
[4] *National Radio Astronomy Observatory, 520 Edgemont Road, Charlottesville, VA 22903-2475, U.S.A*

13 June 2002

ABSTRACT
We have used a deep *Chandra* observation of the central regions of the twin-jet FRI radio galaxy 3C 31 to resolve the thermal X-ray emission in the central few kiloparsecs of the host galaxy, NGC 383, where the jets are thought to be decelerating rapidly. This allows us to make high-precision measurements of the density, temperature and pressure distributions in this region, and to show that the X-ray emitting gas in the centre of the galaxy has a cooling time of only 5×10^7 years. In a companion paper these measurements are used to place constraints on models of the jet dynamics.

A previously unknown one-sided X-ray jet in 3C 31, extending up to 8 arcsec from the nucleus, is detected and resolved. Its structure and steep X-ray spectrum are similar to those of X-ray jets known in other FRI sources, and we attribute the radiation to synchrotron emission from a high-energy population of electrons. *In situ* particle acceleration is required in the region of the jet where bulk deceleration is taking place.

We also present X-ray spectra and luminosities of the galaxies in the Arp 331 chain of which NGC 383 is a member. The spectrum and spatial properties of the nearby bright X-ray source 1E 0104+3153 are used to argue that the soft X-ray emission is mostly due to a foreground group of galaxies rather than to the background broad absorption-line quasar.

Key words: galaxies: active – X-rays: galaxies – galaxies: individual: 3C 31 – galaxies: jets – radiation mechanisms: non-thermal

1 INTRODUCTION

The radio emission from low-luminosity radio galaxies [class I of Fanaroff & Riley (1974), hereafter FRI] is often dominated by bright jets which may extend for many hundreds of kpc on both sides of the central active nucleus. A number of arguments, including observations of superluminal motion in some sources, lead to the conclusion that the jet material moves at relativistic bulk speeds on parsec scales. At large distances from the galaxy, however, the diffuse, relaxed appearance of the jets, their large opening angles, and their brightness symmetry across the nucleus (together with other indicators) suggest that they are trans-sonic or subsonic flows with sub-relativistic speeds. The jets must therefore decelerate on intermediate scales.

There is now a good deal of direct evidence, both from studies of Doppler beaming of individual objects (e.g. Hardcastle et al. 1997; Laing & Bridle 2002a) and samples (Laing et al. 1999) and from independent indicators of source orientation such as depolarization (Morganti et al. 1997) that this deceleration largely happens on scales of $\sim$ 1–10 kpc from the nucleus, corresponding to scales of a few arcseconds at the typical distances of well-studied objects. A plausible mechanism for deceleration is mass loading by the entrainment of thermal material, either by injection from stellar winds within the volume that is traversed by the jet (e.g., Bowman, Leahy & Kommissarov 1996) or by ingestion from the galactic atmosphere across a turbulent boundary layer at the edges of the jet (e.g., Bicknell 1984). All models in which the jet decelerates rapidly by mass loading require the presence of an external pressure gradient to prevent disruption of the jet.

3C 31 is a nearby twin-jet FRI radio galaxy ($z = 0.0169$), hosted by the D galaxy NGC 383, a member of the optical chain Arp 331. 3C 31's bright pair of jets was among the first to be studied in detail at radio frequencies (e.g. Burch 1977; Fomalont et al. 1980). An optical counterpart to the brighter northern jet, first discovered by Butcher, van Breugel & Miley (1980), was not seen in later observations by Keel (1988) and Fraix-Burnet (1991) but appears to be real (Croston et al. in preparation). Recent high-quality radio imaging with the Very Large Array (VLA) allowed Laing & Bridle (2002a) to make detailed models of the velocity field in the jets within 30 arcsec of the nucleus, on the assumption that the jets are intrinsically symmetrical and anti-parallel, so that apparent differences between the brightness and polarization structures arise entirely from differences in Doppler beaming and aberration between approaching and receding flows. They inferred the angle to the line of sight to be 52° with an uncertainty of a few degrees, and

found that the jets decelerate from on-axis speeds of $v/c \approx 0.9$ at 1 kpc from the nucleus to $v/c \approx 0.22$ at 12 kpc along the jet, with slower speeds at the jet edges.

In order for the flaring and recollimation observed in 3C 31 to occur over distances of 1 – 4 kpc, there must be a substantial pressure gradient on this scale. This can only be provided by gas in the hot, X-ray emitting phase. X-ray emission associated with 3C 31 has previously been observed with *Einstein* (Fabbiano et al. 1984) and with the *ROSAT* PSPC and HRI (Trussoni et al. 1997; Komossa & Böhringer 1999; Canosa et al. 1999; Hardcastle & Worrall 1999). Extended X-ray emission from the rich host group of NGC 383 has been seen on arcminute scales, and is well modelled as a thermal plasma with a temperature 1.5 ± 0.1 keV. Komossa & Böhringer fitted it with a β model with $\beta = 0.38$ and core radius 154 arcsec. In addition, all the elliptical galaxies in the chain, including NGC 383 itself, are X-ray sources. Komossa & Böhringer carried out a spectral fit to the PSPC observations of NGC 383 and obtained good fits with a combination of a power law (from the active nucleus) and weaker thermal emission with $kT \sim 0.6$ keV (from unresolved hot gas centred on the galaxy). However, the spatial resolution of the *ROSAT* PSPC, or even the HRI, was insufficient to resolve thermal emission on scales matched to the region of strong deceleration in the jet or to separate it from non-thermal X-ray emission associated with the active galaxy.

In this paper we present a deep *Chandra* observation of the nuclear regions of 3C 31, taken with the aim of accurately constraining the pressure gradient in the inner few arcseconds. We also discuss a newly discovered X-ray jet in 3C 31, and the X-ray emission from the galaxies in the Arp 331 chain and the background source 1E 0104+3153. A companion paper (Laing & Bridle 2002b) presents an analysis of the dynamics of the jets in 3C 31 using the kinematic model of Laing & Bridle (2002a), the external density and pressure distributions from our *Chandra* observations, and a conservation-law approach based on that of Bicknell (1994). There it is shown that the jets can indeed be decelerated by mass injection and recollimated by the external pressure gradient, and the variations of internal pressure and density along them are inferred.

Throughout the paper we use a cosmology with $H_0 = 70$ km s^{-1} Mpc^{-1} and $q_0 = 0$, so the linear scale is 340 pc arcsec^{-1} at the redshift of the host galaxy.

2 THE OBSERVATIONS

We observed 3C 31 for 44410 s with the *Chandra* ACIS-S on 2000 November 6th. 3C 31 was positioned near the aim point on the back-illuminated S3 CCD. There were no high-background intervals or aspect excursions during the observation, so no temporal filtering of the data was required. We reprocessed the observation using CIAO version 2.1 to generate a new level 2 events file containing events with the standard set of event grades but with the 0.5-pixel randomization removed.

Fig. 1 shows an image of the inner regions of 3C 31, made from all events with energies between 0.5 and 7.0 keV. (Throughout the paper, images and spectral fits use the events in this energy range.) Extended emission on scales of the host galaxy, and an X-ray core and jet, are detected. Their spectral and spatial properties are discussed in the following sections. Spectra were extracted and corresponding response matrices constructed using CIAO, and model fitting was carried out in XSPEC. In all cases the extracted spectra were grouped so that each fitting bin had > 20 counts. Errors quoted throughout are the 1σ value for one interesting parameter, unless otherwise stated. All power-law indices are the energy index or spectral index, α, defined in the sense that the flux density $S \propto \nu^{-\alpha}$.

3 THE X-RAY CORE

In an extraction circle with radius 1.5 arcsec centred on the X-ray nucleus of 3C 31, using a source-centred background annulus with radii between 2 and 5 arcsec (excluding jet emission), there are 835 ± 33 net counts. The spectrum of this emission is very poorly fitted either with a single power-law model ($\chi^2/n = 84/32$, $\alpha = 1.6 \pm 0.2$, $N_H = (1.8 \pm 0.4) \times 10^{21}$ cm^{-2}) or with a thermal (MEKAL) model ($\chi^2/n = 90/31$, $kT = 0.98 \pm 0.11$, $N_H = (1.4 \pm 0.3) \times 10^{21}$ cm^{-2}, abundance 0.04). It is better fitted ($\chi^2/n = 22/30$) with a combination of the two: fixing the absorbing column for the thermal component at the Galactic value (5.53×10^{20} cm^{-2}) and the abundance to 0.2 solar (see section 7), the best-fitting power-law model has an intrinsic absorbing column at the redshift of the galaxy of $(1.5^{+2.2}_{-1.4}) \times 10^{21}$ cm^{-2} and a power-law index of $0.52^{+0.29}_{-0.16}$, while the thermal component has $kT = 0.66 \pm 0.04$ keV and contributes 55 ± 10 per cent of the observed emission at 1 keV, or 450 ± 80 net counts. The unabsorbed 1-keV flux density of the power-law component of the core in this model is 9 ± 2 nJy. The radio-to-X-ray spectral index, $\alpha_{\rm RX}$, between the arcsecond-scale nuclear radio emission (using the 8.4-GHz flux density of 91 mJy) and the power-law component of the core X-ray emission is 0.94 ± 0.01, which is similar to the values for the B2 radio sources observed by Worrall et al. (2001).

When we use an extraction region matched to that of Canosa et al. (1999), who determined a flux density of 64 nJy for the nuclear region of the source from *ROSAT* HRI data, we find that the *Chandra* X-ray flux in the *ROSAT* band is consistent. There is thus no evidence for X-ray variability of 3C 31's nucleus, though this is a weak constraint; variability at the level of tens of per cent in the net count rate would not have been detectable given the *ROSAT* uncertainties, so that the non-thermal component of the core could have varied by ~ 50 per cent between the *ROSAT* and *Chandra* observations. The larger *ROSAT* flux density quoted by Canosa et al. includes emission from the thermal component of the core, from the X-ray jet (Section 4) and from the extended thermal emission around 3C 31 (Section 7).

The lack of strong absorption of the power-law component of 3C 31 (there is no more absorption than would be expected given the observed dust features in *Hubble Space Telescope* images) is consistent with the results we have obtained for other FRI radio galaxies (Worrall et al. 2001, Hardcastle et al. 2001). These results imply that the line of sight to the nuclear power-law component in these objects does not intersect the kind of 'torus' inferred from observations of some FRII radio sources (e.g., Ueno et al. 1994). Similar considerations apply to the nuclear optical emission observed from the host galaxies of FR I sources (Chiaberge et al. 1999, Hardcastle & Worrall 2000). Two possibilities can be envisaged: a) the nuclear optical and X-ray emission originates mainly in the jet on scales larger than the torus, and is therefore not absorbed; or b) there is no torus, in which case some or all of the observed X-ray emission could originate in the active nucleus itself (from the accretion disc and environs). We have argued elsewhere (e.g., Canosa et al. 1999; Hardcastle & Worrall 2000) for the former possibility, based on the observed correlation between radio and X-ray core emission, which suggests that the nuclear soft X-ray emission originates in the jets, presumably on pc- to 100-pc scales.

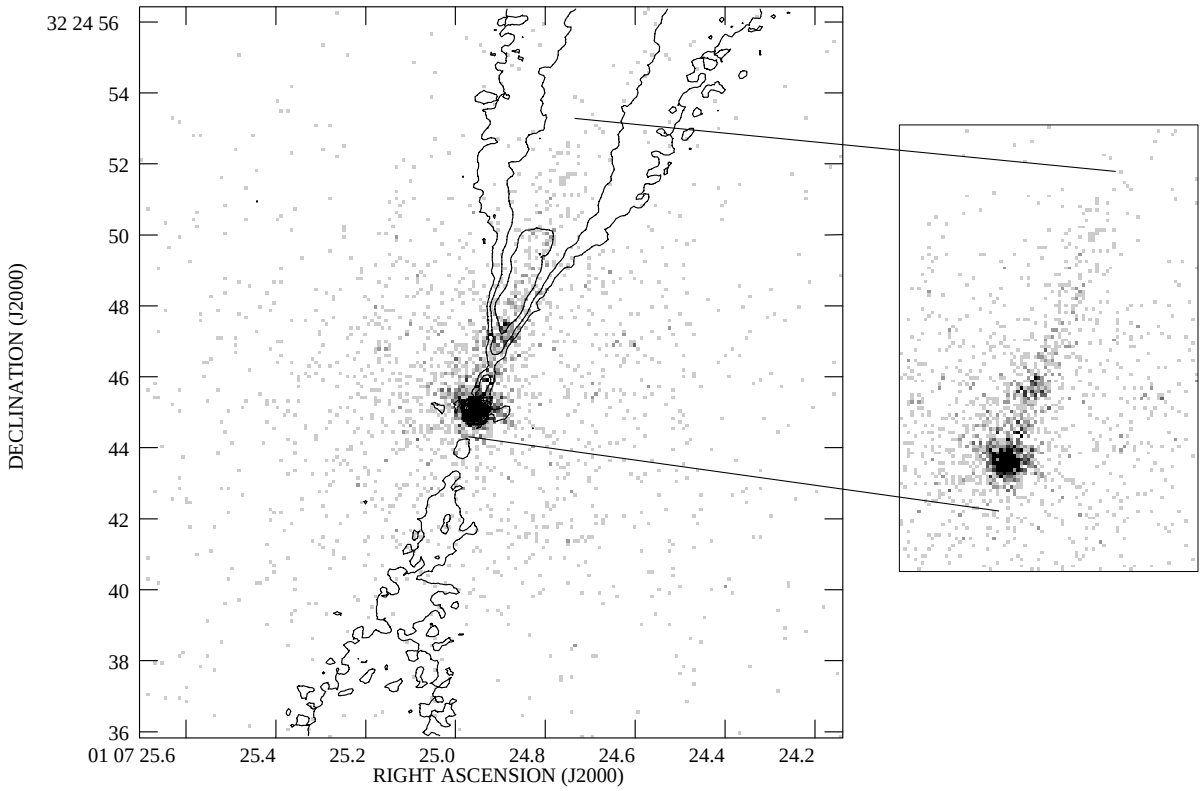

Figure 1. *Chandra* image of the inner regions of 3C 31. The greyscale has a pixel size of 0.0946 arcsec, with black being 5 counts per pixel. Left: superposed are contours from an 8.5-GHz radio map at a resolution of 0.25 arcsec, at $20 \times (1, 4, 16, \ldots)$ μJy beam^{-1}. The core X-ray centroid has been aligned with the radio core position as discussed in the text. Right: the X-ray jet alone, on the same scale.

However, we note that infra-red observations have led Whysong & Antonucci (2001) and Perlman et al. (2001) to infer that there is no torus (or, more generally, no heavily absorbed nuclear component above a certain bolometric luminosity) in one FRI radio galaxy, M87. Most Chandra observations of FRI sources do not show any evidence for a heavily absorbed nuclear X-ray component, although Birkinshaw et al. (in preparation) will report on a detection of an absorbed nuclear component in NGC 4261. X-ray observations are therefore consistent with the absence of a torus in some sources, in turn implying that we cannot rule out the possibility of a contribution from the active nucleus to the observed nuclear X-ray emission in 3C 31. (Jet-related X-rays must still dominate in a substantial fraction of the FR I population to explain the observed radio/X-ray correlation.) If the X-rays from 3C 31's nucleus *do* originate in the small-scale jet, then their flat spectrum is most consistent with an inverse-Compton model, as predicted by Hardcastle & Worrall (2000). However, the other *Chandra* evidence on this point is inconsistent: M87 (Wilson & Yang 2002), 3C 66B (Hardcastle et al. 2001) and the three objects studied by Worrall et al. (2001) have all exhibited steeper nuclear spectra, $\alpha \approx 1$, though in some cases the errors were large. We defer detailed discussion of the radio to X-ray nuclear spectra of FRI sources to a future paper.

Using the default *Chandra* astrometry, the core centroid is displaced by about 0.13 arcsec north of the accurately known radio core position. This offset is within the known uncertainty in *Chandra* source positions, so we have corrected the X-ray positions to remove the displacement. However, since there is a substantial contribution to the X-ray counts in the nuclear region from thermal emission which may not be centred on the active nucleus, the accuracy of the alignment between the radio and X-ray frames is probably no better than about 0.05 arcsec.

4 THE X-RAY JET

X-ray emission is clearly detected from the brighter, northern radio jet of 3C 31, extending about 8 arcsec from the nucleus. Fig. 1 shows that most of this emission corresponds to the well-collimated inner region of the jet at radio wavelengths, with the peak intensity in the X-ray emission occurring where the radio emission begins to brighten and decollimate. A rectangular region (6.5 arcsec by 1.7 arcsec) around the jet but avoiding the core, with background taken from adjacent identical rectangles, contains 368 ± 35 net counts. A power-law model of the spectrum, assuming Galactic absorption, gives a good fit to the data ($\chi^2/n = 7.3/13$) with $\alpha = 1.09 \pm 0.16$. The improvement in the fit produced by allowing the absorbing column to vary is not significant on an F-test. The spectrum can also be fitted adequately ($\chi^2 = 11.5/13$) with a thermal model with $kT = 2.3^{+0.7}_{-0.3}$ keV, Galactic absorption and a (fixed) abundance of 0.2 solar. On the preferred power-law model, the unabsorbed flux density of the jet at 1 keV is 7.3 ± 0.5 nJy.

Two X-ray jets in FRIs, in the nearby objects M87 (Harris et al. 1997) and Centaurus A (Turner et al. 1997) were known before the launch of *Chandra*, but *Chandra* observations have resulted in the detection of a number of new FRI X-ray jets, including those in B2 0206+35 and B2 0755+37 (Worrall, Birkinshaw & Hardcastle 2001) and 3C 66B (Hardcastle, Birkinshaw & Worrall 2001). In the latter paper we argued that the X-ray emission from all known FRI

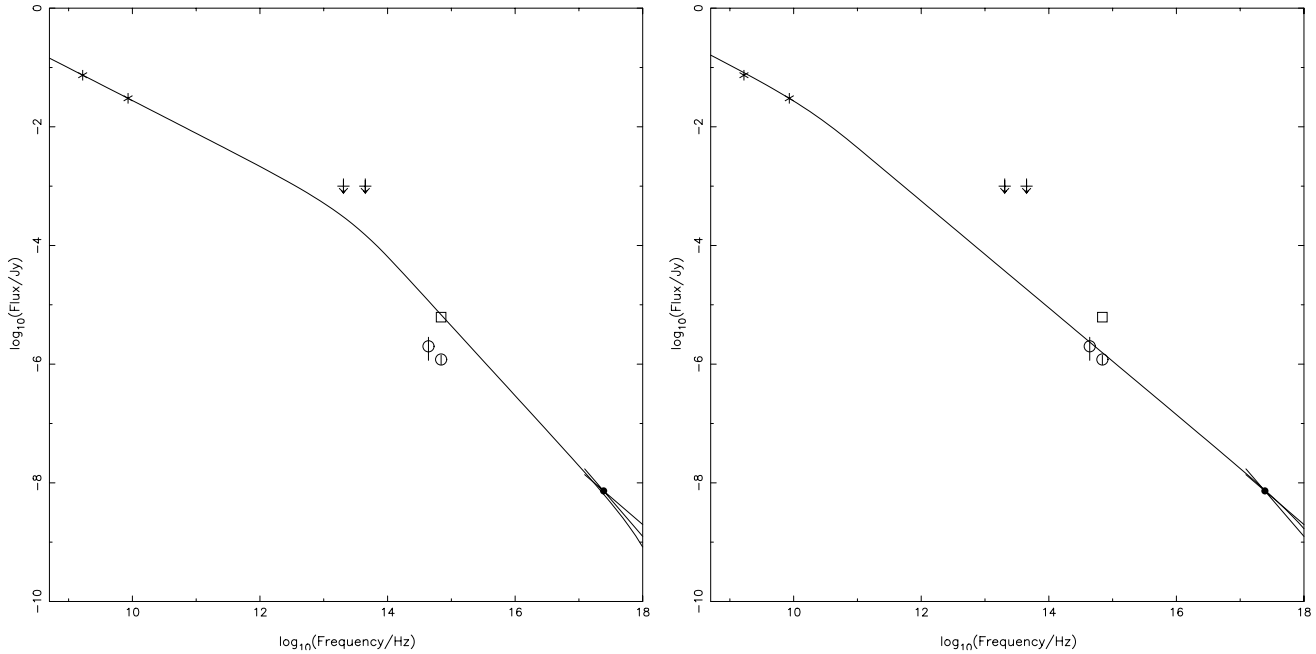

Figure 2. The radio-to-X-ray spectrum of the jet of 3C 31, based on the whole 6-arcsec region of the jet detected with *Chandra*. Radio points (stars) are taken from the data of Laing & Bridle (2002a); the infra-red data points (crosses) are upper limits derived from our ISO observations (Tansley et al. 2002); the high optical data point (box) is the flux density of Butcher et al. (1980), while the lower optical data points (open circles) are the data of Croston et al. (in preparation); the filled circle is the X-ray flux density reported in the text. The 'bow tie' around the X-ray flux density illustrates the 1σ range of spectral index in the power-law fit to the jet spectrum. The solid lines show broken power-law synchrotron models of the kind discussed in the text: left, the model fitting the Butcher et al. optical flux, with a spectral break in the infra-red; right, the model fitting the Croston et al. optical fluxes, with a break in the mm-wave region.

X-ray jets was consistent with being synchrotron emission from the high-energy tail of the electron population responsible for the radio emission. The radio-to-X-ray ratio and X-ray spectral index of 3C 31's jet are very similar to those observed in other sources, suggesting that a synchrotron model can be applied to 3C 31 as well. The steep spectrum of the X-ray emission would not be expected in an inverse-Compton model for the jet emission, and for magnetic fields close to equipartition standard inverse-Compton models (where the scattered photon population is the synchrotron photons or the CMB) underestimate the observed X-ray flux density by three to four orders of magnitude. The well-constrained jet speeds and angle to the line of sight (Laing & Bridle 2002a) mean that beamed inverse-Compton models (e.g. Tavecchio et al. 2000) do not apply here. As we argued in the case of 3C 66B, light from the hidden BL Lac object in the core of the AGN probably dominates the photon density in the jet. In this case, we could produce the observed X-ray flux density (but not the spectrum) if the hidden BL Lac (whose spectrum is modelled here as a simple power law from radio through to optical) had an effective flux density, as seen from the jet direction, of about 1000 Jy in the radio. This is very large, and requires high beaming Lorentz factors (~ 7) in the presumed BL Lac nuclear jet, at 52° to the line of sight, in order not to over-produce the observed radio core emission. For more plausible values of the hidden BL Lac flux density, substantial departures from equipartition are still required to produce the observed X-ray emission by the inverse-Compton mechanism, and the departures become even larger if the expected relativistic motion of the jet away from the nucleus is incorporated in the models. Because of this, and of the steep X-ray spectrum, we favour a synchrotron model for the X-ray emission from the jet.

The 3C 31 jet's optical properties are less well known than in M87 and 3C 66B. As discussed in Section 1, several studies have failed to detect any optical emission at all, while Butcher et al. (1980) claimed a significant detection. Large uncertainties arise because of the central dust lane and the bright rim of stellar emission around it (Martel et al. 1999), which unfortunately cross the brightest part of the radio jet. Most recently, Croston et al. (in prep.) have measured a flux density for the optical emission *outside* this rim structure. If we scale up their flux to match our X-ray extraction region, using the ratio of radio flux densities inside and outside the X-ray region to account for the optical emission obscured by the dust lane and its rim, we obtain net flux densities in the R and B bands of 2.0 ± 0.8 and 1.2 ± 0.3 μJy respectively, although this scaling procedure assumes that there is no variation in radio-optical spectral index along the jet. As Fig. 2 shows, the uncertainties in the optical flux lead to uncertainties in the best-fitting synchrotron model: if we adopt the value of Butcher et al. (1980) we can fit a model which is quite similar to that seen in M87 and 3C 66B, in which the spectrum breaks from its radio value of $\alpha = 0.55$ somewhere in the infra-red by $\Delta\alpha = 0.63$, whereas if we use the values of Croston et al. we require a smaller spectral break ($\Delta\alpha = 0.35$) which occurs at much lower frequency in order to accommodate the X-ray, optical and radio data.

Although the SED is currently uncertain, a synchrotron model of some sort is certainly viable for 3C 31. Given the very short synchrotron lifetimes of the X-ray emitting electrons, such a model requires *in situ* acceleration of at least the high-energy electron population. One possible source of energy for particle acceleration, at least in the outer regions of the X-ray jet, is the strong bulk jet deceleration inferred by Laing & Bridle (2002a).

As Fig. 1 shows, both the X-ray and radio emission from the jet are comparatively smooth, with little sign of the knotty structure seen in M87 or 3C 66B. However, there is a clear X-ray peak at just over 2 arcsec from the core, containing about 100 counts in total,

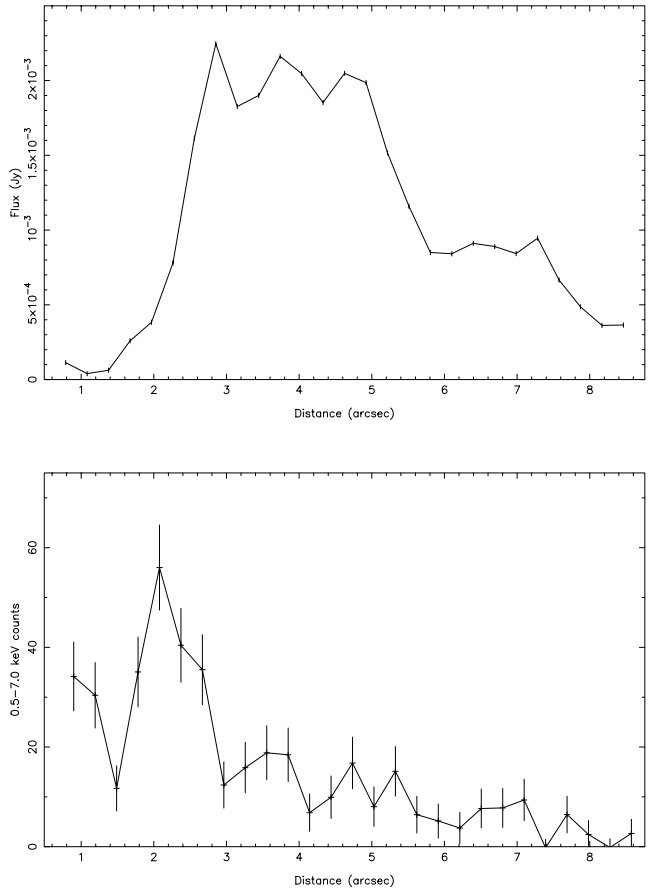

Figure 3. Profiles of the jet in the radio (upper panel) and X-ray (lower panel). Profiles were made using the maps of Fig. 1, extracting all the emission from a series of rectangles of 0.3 arcsec by 2.0 arcsec (long axis perpendicular to the jet axis). Background subtraction was carried out using adjacent rectangles for each bin. The innermost two bins of the X-ray profile are dominated by emission from the X-ray nucleus. Errors on the points on the X-ray profile are 1σ; note that the X-ray data points are not independent, since the sampling along the jet axis is smaller than the resolution of *Chandra* (~ 0.6 arcsec FWHM). The restoring beam used in the radio maps was 0.25 arcsec FWHM, so that the radio points are effectively independent. However, the errors on these points are 1σ based on the off-source noise, and so are lower limits on the actual errors.

which lies in the region where the jet's radio flux increases steeply as a function of distance from the core. The knot can be seen in the X-ray profile along the jet shown in Fig. 3 and is associated with the well-collimated inner region defined by Laing & Bridle (2002a). In 3C 66B, Centaurus A and M87 (Hardcastle et al. 2001; Kraft et al. 2002; Wilson & Yang 2002) unexpectedly strong X-ray emission is seen from the radio-weak inner parts of the jet, and it seems plausible that we are seeing a similar phenomenon in 3C 31. In the case of 3C 66B, we argued that a difference in the particle acceleration process (or conceivably a different emission mechanism) was required in the inner jet. (This sort of offset between radio and X-ray peaks is expected in a nuclear inverse-Compton model, but such models are not favoured here for the reasons discussed earlier.) The flow in the inner 3 arcsec of the jet is inferred by Laing & Bridle (2002a) to have a fast component ($v/c \approx 0.8$ – 0.9) together with much slower material, although the transverse velocity profile is unresolved; there are therefore at least two possible components of the jet from which this excess X-ray emission could originate. It is tempting to relate the excess in some way to the reconfinement shock at which the internal pressure of the jet falls below the pressure of the external medium, which, as discussed by Laing & Bridle (2002b), is expected to occur somewhere in this region. But in the absence of a detailed model for the velocity structure in this faint part of the jet we cannot give a definitive explanation for this component.

It is important to note that optical and X-ray jet emission is also associated with the flaring region defined by Laing & Bridle (2002a), between 2.5 and 8.2 arcsec from the nucleus, where deceleration is inferred to start. No X-ray emission is detected from the outer region (> 8.2 arcsec from the nucleus). In the flaring region, the radio-to-X-ray ratio appears constant within the errors. There is no evidence for a spectral difference between the inner X-ray jet (< 2.5 arcsec) and the outer jet (> 2.5 arcsec), though the errors are large. Nor is there any radio spectral difference between the flaring region of the jet and the rest. Transverse profiles taken across the inner and flaring regions (Fig. 4) also show little difference between them; there is no strong evidence that either of the regions is more centrally peaked in the X-ray than in the radio.

No X-ray emission is detected from the counterjet. The radio jet-to-counterjet ratio, $R_{\rm radio}$, is ~ 10 in the inner 6 arcsec, so we might have expected to see ~ 40 counts from the counterjet if the ratio were the same in the X-ray. In a relativistic beaming model for the synchrotron radiation, however, the steeper spectrum of the X-ray emission gives rise to a greater K-correction, so that the X-ray and radio jet-counterjet ratios should not be the same. The predicted $R_{\rm X}$ is $R_{\rm radio}^{(2+\alpha_{\rm X})/(2+\alpha_{\rm radio})}$, or about 16, leading to a prediction of about 25 X-ray counts in the X-ray counterjet. Our 3σ upper limit on X-ray counts from the the counterjet region is about 30 counts. The jet-to-counterjet ratio in the X-ray is therefore consistent with relativistic beaming of an intrinsically identical synchrotron X-ray jet and counterjet; there is no evidence for an intrinsic difference between the X-ray emission on the jet and counterjet sides.

5 THE CHAIN GALAXIES

All the bright galaxies of the Arp 331 chain, including NGC 383's companion galaxy NGC 382, are detected in the *Chandra* observation (Fig. 5). We have extracted spectra for each object using 12-arcsec source circles centred on the galaxy, with background taken from annuli between 12 and 15 arcsec; we use matched source regions to facilitate comparisons between sources. The resulting count rates and spectral fits are tabulated in Table 1. We tried to fit a power-law with Galactic absorption or a MEKAL model with Galactic absorption and abundance 0.2 solar to each spectrum. If neither model gave a satisfactory fit we allowed the absorbing column or the abundance to vary, or fitted a model combining thermal and power-law components. We tabulate only satisfactory fits, with $\chi^2/n \lesssim 2$.

Although the luminosities derived for the companion objects are somewhat model-dependent, they are in broad agreement with the *ROSAT*-derived values of Trussoni et al. (1997) and Komossa & Böhringer (1999). The luminosities are all in the general range expected for isolated coronae of early-type galaxies (Forman, Jones & Tucker 1985) but several of the spectra are either best fitted with non-thermal models or have a non-thermal component. This may indicate a contribution from discrete X-ray sources, such as binaries, in these galaxies, though the required luminosities ($\sim 10^{41}$ ergs s^{-1}) are rather higher than expected for normal binary num-

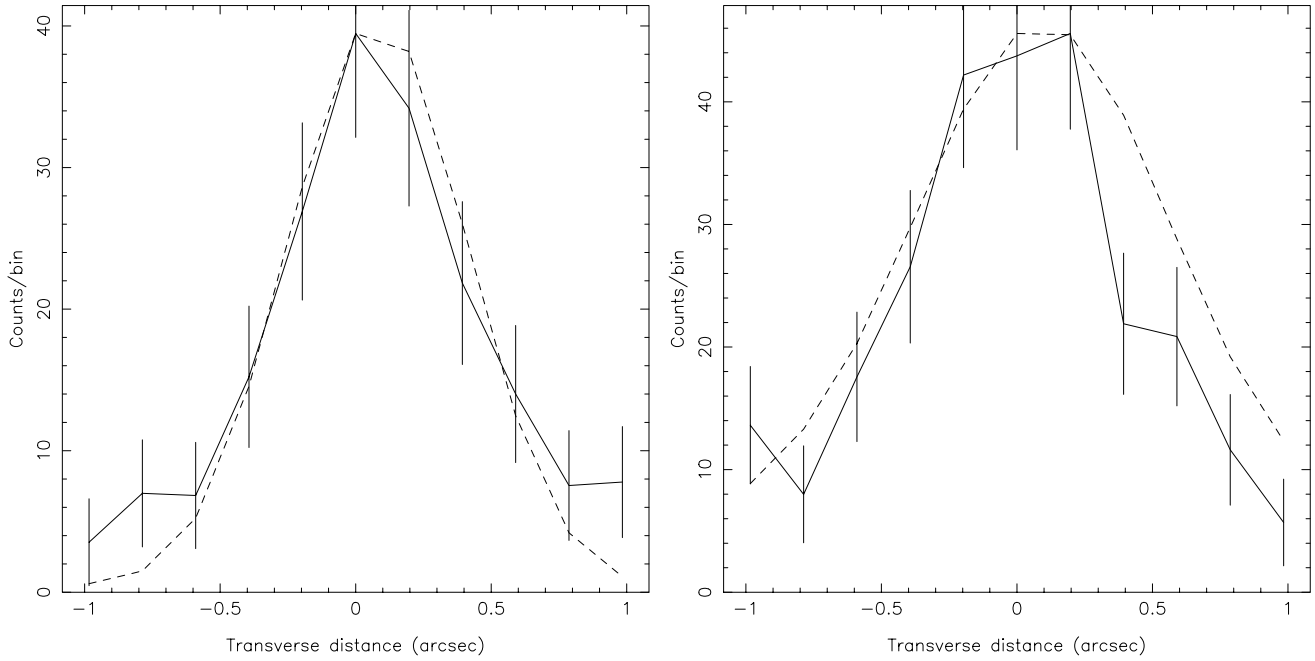

Figure 4. Transverse slices across the jet in X-ray (solid line) and radio (dashed line). Left: the inner jet (1.5 to 2.5 arcsec from the nucleus). Right: the flaring region of the jet (2.5 to 8 arcsec from the nucleus). Each bin represents a rectangle 0.2 arcsec wide. The zero of the abscissa is on the ridge line of the jet and the positive direction is to the SW. The radio data, from an 8.4-GHz image convolved to a resolution of 0.65 arcsec (roughly matching the *Chandra* resolution), is plotted for comparison, scaled so that the maxima of the two curves are the same.

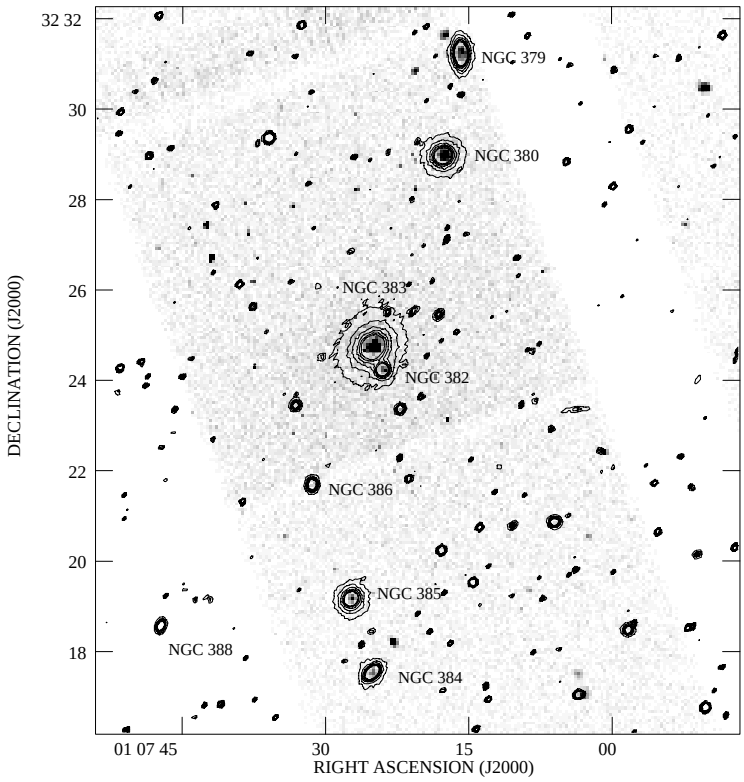

Figure 5. *Chandra* image of the galaxies in the Arp 331 chain; pixels are 3.94 arcsec on a side. Overlaid are contours from the red Digital Sky Survey-2 plates. No exposure correction has been applied, and *Chandra* chip boundaries are visible; NGC 379, 380, 383 (3C 31) and 382 lie on the S3 chip, while NGC 385 and 384 lie on the front-illuminated S2 chip.

Table 1. X-ray data for the Arp 331 galaxies

Source	Count rate (10^{-3} counts s^{-1})	Model type	Model parameters	χ^2/n	L_{model}, 10^{41} erg s^{-1} (0.1–2.4 keV)
NGC 379	6.1 ± 1.0	MEKAL, free abundance	$kT = 0.96 \pm 0.15$ keV, abundance = 0.04 ± 0.03	8.6/7	3.0
		power-law	$\alpha = 1.6 \pm 0.3$	12.1/8	6.6
NGC 380	24.2 ± 1.2	MEKAL, free absorbing column	$kT = 0.59 \pm 0.02$ keV, $N_{\rm H} = (19 \pm 3) \times 10^{20}$ cm^{-2}	42.9/33	12.2
NGC 383	54.3 ± 1.5	MEKAL + power-law (32%)	$kT = 0.67 \pm 0.02$ keV, $\alpha = 0.53 \pm 0.08$	113/71	16.4
NGC 382	3.4 ± 1.0	MEKAL, free abundance	$kT = 0.72 \pm 0.2$ keV, abundance < 0.02	9.5/7	1.8
		power-law	$\alpha = 1.9 \pm 0.3$	10.1/8	4.7
NGC 385	4.1 ± 1.0	MEKAL + power-law (39%)	$kT = 0.4 \pm 0.3$ keV, $\alpha = 0.2 \pm 0.6$	4.1/5	2.1
NGC 384	2.9 ± 1.0	power-law	$\alpha = 1.1 \pm 0.4$	5.7/3	2.1

Luminosities are unabsorbed, and are calculated assuming that all objects are at the assumed distance of NGC 383/3C 31 (luminosity distance 73.0 Mpc); they are derived from 12 arcsec (4.1 kpc) source circles. We use the *ROSAT* energy band to aid comparison with the results of Komossa & Böhringer (1999). Unless otherwise stated, abundances used are 0.2 solar and the absorbing column is Galactic. For multi-component models, the percentage quoted for the power-law component is the fraction of counts between 0.5 and 7.0 keV contributed by the model.

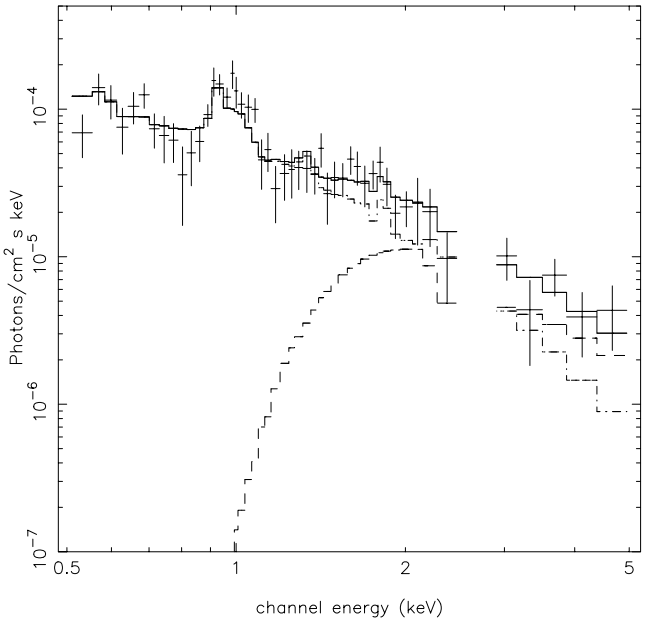

Figure 7. The spectrum of 1E 0104+3153 with the best-fitting model, consisting of a MEKAL model and heavily absorbed power-law component, as described in the text. The data at around 2.7 keV and above 5 keV were excluded from the fit because these bins contained few counts after background subtraction.

bers. In the case of NGC 383 the non-thermal component is attributed to the AGN (Section 3).

6 1E 0104+3153

The *Einstein* source 1E 0104+3153 lies 16.6 arcmin to the SW of 3C 31, and is detected on the back-illuminated ACIS-S1 chip. The X-ray source is close on the sky both to a $z = 2.2$ broad absorption-line (BAL) quasar and to a $z = 0.11$ elliptical galaxy in a group (Stocke et al. 1984; Fig. 6) and so the origin of the X-ray emission is not clear. Komossa & Böhringer (1999) obtained a more accurate position for the X-ray source with the *ROSAT* HRI, but could not resolve the ambiguity in the identification. At this distance off-axis, the *Chandra* PSF is broad, with a half-energy radius of ~ 15 arcsec. The spatial resolution of *Chandra* therefore does not allow us to identify the X-ray source; in fact, the *Chandra* position of the source centroid, at (J2000) RA $01^{\rm h}06^{\rm m}58^{\rm s}.737$, Dec. $+32^\circ09'25''.15$, lies in between the optical positions of the BAL object and the galaxy, which are RA $01^{\rm h}06^{\rm m}58^{\rm s}.756$, Dec. $+32^\circ09'18''.03$ and RA $01^{\rm h}06^{\rm m}58^{\rm s}.978$, Dec. $+32^\circ09'28''.02$ respectively (Stocke et al. 1984), at 7 and 4 arcsec away from the centroid. The source looks more extended than two nearby bright sources on the same chip, which would tend to favour an identification with the emission from the $z = 0.11$ group. The large number of counts in the *Chandra* observation, 1834 ± 82 in a 1-arcmin source circle with background between 1 arcmin and 75 arcsec, allow us to make a good determination of the source spectrum. A power-law model with absorption fixed to the Galactic value gives a poor fit ($\chi^2/n = 93/47$, $\alpha = 0.7$). With excess absorption the fit is significantly improved ($\chi^2/n = 80/46$, $N_H = 2 \times 10^{21}$ cm^{-2}, $\alpha = 1.3 \pm 0.2$), but there are still clear residuals at around 1 keV. The data are also consistent with a MEKAL model at the redshift of the elliptical galaxy, with Galactic absorption and fixed abundance 0.35; in this case we obtain $kT = 2.5 \pm 0.3$ keV, with $\chi^2/n = 56/47$. However, the best fits to the data are obtained with a combination of a MEKAL model at $z = 0.11$ and an absorbed power-law; we obtain $\chi^2/n = 39/44$ with Galactic absorption, a temperature $kT = 1.8 \pm 0.1$ keV for the thermal component, and for the absorbed power law a column of $(6 \pm 4) \times 10^{23}$ cm^{-2} at the redshift of the quasar and $\alpha = 1.9 \pm 1.3$. In this model (Fig. 7), the thermal plasma from the group contributes almost all the soft X-ray emission, while the BAL power-law contributes to the high-energy tail, giving rise to ~ 10 per cent of the total counts between 0.5 and 5 keV. Such a high column density is not unexpected for a BAL object (e.g., Green et al. 1995) and the unabsorbed rest-frame 2–10 keV flux would be 4×10^{-13} ergs cm^{-2}, leading to a luminosity of 2×10^{46} ergs s^{-1}, not implausible for a quasar. The temperature of the thermal component is consistent with that measured by Komossa & Böhringer, and its luminosity in our extraction region, assuming $z = 0.11$, is $\sim 10^{43}$ ergs s^{-1}, which is consistent with the temperature-luminosity relation for groups (e.g., Worrall & Birkinshaw 2000). The statistics of the X-ray observation, given the large *Chandra* PSF at this off-axis radius, are not good enough to distinguish a significant offset between the centroids of the X-ray source in the soft and hard bands, so we cannot be certain that the quasar contributes to the hard emission. But, given the extended ap-

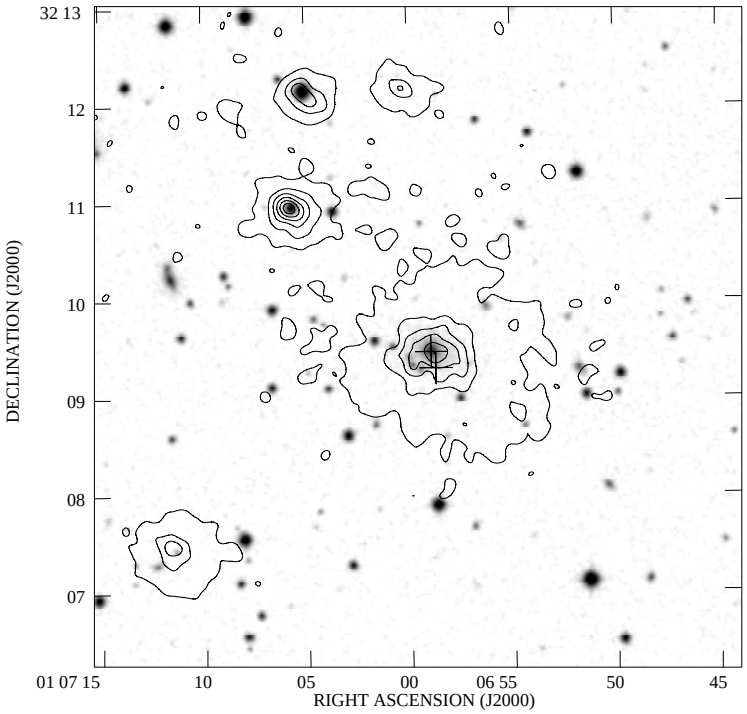

Figure 6. DSS image of the region around 1E 0104+3153. Overlaid are contours of the *Chandra* image, smoothed with a Gaussian kernel with a FWHM of 8 arcsec; contour levels are at $0.04 \times (4, 10, 15, 20 \ldots)$ counts arcsec^{-2}. The lowest contour is at the 3σ level, determined as specified by Hardcastle (2000); 1E 0104+3153 appears significantly more extended than other X-ray detected objects in the field. The two X-ray sources to the NE appear to be identified with stars. Crosses mark the positions of the elliptical galaxy (northern object) and the BAL quasar, given by Stocke et al. (1984).

pearance of the source and the lack of X-ray variability reported by Komossa & Böhringer (1999), we suggest that the *Chandra*-band X-ray emission from this source is dominated by the hot gas in the $z = 0.11$ group.

7 THE EXTENDED EMISSION

The arcmin-scale extended emission discussed by Trussoni et al. (1997) and Komossa & Böhringer (1999) is visible in our data mainly as an increased background around 3C 31. However, there is also a clear extended halo around the core and jet of 3C 31 (Fig. 1), which is detectable by eye out to about 30 arcsec from the nucleus, though the bulk of the counts lie within 10 arcsec. The 0.4–5.0 keV luminosity of this component within 30 arcsec (10 kpc) is around 10^{41} ergs s^{-1}, so that it is comparable to the galaxy-scale gas components seen with *Chandra* around other FRI radio galaxies (Worrall et al. 2001).

To characterize the extended emission spatially we used software based on the FUNTOOLS package to extract a radial profile directly from the 0.5–7.0 keV events dataset. The profile was centred on the nucleus, and excluded all detected background point sources, as well as the pie slice between position angles of 320 and 360 degrees (to avoid contamination from jet emission). The radial profile extended out to 110 arcsec from the core, with background being taken between 110 and 130 arcsec; the size of the radial-profile region was restricted by the requirement that it lie only on the S3 chip. Small changes in the *Chandra* PSF on these angular scales do not significantly affect our analysis. Exposure correction was applied to the radial-profile data using an exposure map calculated at the peak energy of the dataset, 0.83 keV, as described in

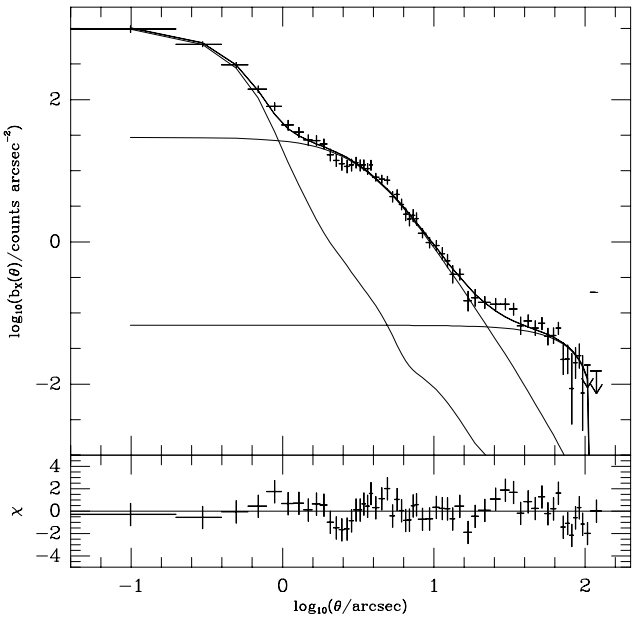

Figure 8. The radial profile of the extended emission around 3C 31, with the best-fitting model as described in the text.

the CIAO 2.1 'science threads'. The resulting radial profile (Fig. 8) was fitted with a model consisting of a point source (we use the PSF parametrization of Worrall et al. 2001), a free β model, and a β model with $\beta = 0.38$ and core radius 154 arcsec, corresponding to the fit of Komossa & Böhringer (1999) to the PSPC data.

Table 2. Best-fitting temperatures and abundances for regions of 3C 31's small-scale thermal emission

Region	kT (keV)	Abundance	χ^2/n	Deprojected kT (keV)
2.5–15 arcsec	0.75 ± 0.04	0.16 ± 0.04	46.6/33	–
2.5–5 arcsec	0.63 ± 0.03	0.12 ± 0.06	18.5/13	0.60 ± 0.04
5–10 arcsec	0.78 ± 0.05	0.15 ± 0.06	6.7/9	0.76 ± 0.05
10–20 arcsec	1.3 ± 0.3	0.13 ± 0.1	0.1/3	1.1 ± 0.2

[We choose to follow Komossa & Böhringer rather than Trussoni et al. (1997) because the former authors used an improved exposure correction in the PSPC analysis (Feretti, private communication).] Small changes in the *Chandra* PSF over the off-axis distances involved do not significantly affect our analysis. The best-fitting parameters of the free β model were $\beta = 0.73 \pm 0.07$, $r_c = 3.6 \pm 0.7$ arcsec (errors are 1σ for 2 interesting parameters), with $\chi^2/n = 58.37/55$. The unresolved core component contained 761 ± 10 counts and the central normalization of the inner β model was 33 ± 3 counts arcsec^{-2}, while the larger β model had a central normalization of 0.25 ± 0.02 counts arcsec^{-2}.

The central count density of the β model means that we would expect to see no more than around 200 counts from extended thermal emission in the 1.5-arcsec extraction radius around the core discussed in section 3, whereas the spectral fits to the core implied that there was nearly twice this amount of thermal emission. These facts can be reconciled if we hypothesize that there is an unresolved, dense component of thermal emission close to the active nucleus. This additional component, if present, does not affect the dynamical analysis of Laing & Bridle (2002b), which starts at a distance of 2.5 arcsec from the nucleus, and so we neglect it in what follows.

We initially fitted a single thermal model to the spectrum of the extended emission between 2.5 and 15 arcsec, using as background an annulus between 20 and 30 arcsec from the core and excluding the quadrant containing the jet. This region contains 820 ± 37 net counts. Its spectrum is adequately fitted using a MEKAL model with Galactic absorption and free abundance, as shown in Table 2. The temperature of 0.75 ± 0.04 keV is in good agreement, within the errors, with the temperature of ~ 0.6 keV estimated for the small-scale thermal component by Komossa & Böhringer (1999).

However, when we divided this region into three smaller annuli, we found significant differences between the temperatures of the three regions (Table 2). There appears to be good evidence for a temperature gradient in this small-scale thermal emission, although the best-fitting abundances are consistent. Assuming that there is no abundance gradient, we then used the β model fit to carry out a simple deprojection of the three annuli, fitting three temperatures to the inner annulus, two to the middle annulus and one to the outer annulus, and scaling the emission measures of the extra components in the inner annuli suitably to take account of the spatial variation as parametrized by the β model. We obtained good fits with an abundance of 0.19 ± 0.04 and deprojected temperatures as tabulated in Table 2. We adopt these temperatures, together with the temperature $kT = 1.5 \pm 0.1$ keV obtained from the *ROSAT* data at larger radii by Komossa & Böhringer (1999), to parametrize the temperature gradient in the thermal emission, fitting a model of the form

$$kT(r) = \begin{cases} kT_0 + cr & r < r_m \\ kT_L & r > r_m \end{cases}$$

Table 3. Properties of the β models fit to the data

Model	β	r_c (arcsec)	Central normalization (m^{-3})
Inner	0.73	3.6	1.8×10^5
Outer	0.38	154	1.9×10^3

where we take $kT_L = 1.5$ keV. For r in arcsec, the best-fitting values are $c = 0.047 \pm 0.015$ keV arcsec^{-1} and $kT_0 = 0.42 \pm 0.11$ keV (since the slope and intercept are strongly correlated, the errors are 1σ for two interesting parameters). For the best-fitting values we infer $r_m = 22.8$ arcsec.

The relationship between volume-weighted emission measure and *Chandra* counts in the 0.5–7.0 keV energy band is not a strong function of temperature at temperatures around 1 keV, though it is quite sensitive to abundance. Since we see no evidence for an abundance gradient, we can safely assume that there is no strong radial dependence of the count density on spectral parameters; it therefore simply traces the density of X-ray-emitting gas, and the analysis of Birkinshaw & Worrall (1993) applies. Making the approximation that the count density as a function of radius can be written as the *sum* of the count densities from the two β models involved, we use the results of Birkinshaw & Worrall to determine the proton density and, by using the observed temperatures, the pressure as a function of radius in the small-scale X-ray-emitting gas. In Fig. 9 we plot the inferred density and pressure. We tabulate the properties of the two β models in Table 3.

Fig. 10 shows the inferred cooling time, calculated using the MEKAL model to take account of the fact that line cooling is important at these temperatures. At $r = 0$ the cooling time is only 5×10^7 years, and it is less than the Hubble time for $r \lesssim 35$ arcsec (12 kpc). The unresolved thermal component discussed above would be expected to have an even shorter cooling time. The central regions of the thermal environment of 3C 31 are therefore expected to be cooling significantly, an expectation which is qualitatively consistent with the observed decrease in temperature with decreasing radius. Short cooling times are often inferred on kpc scales in elliptical galaxies, but it is interesting that the cooling times we derive for 3C 31 mean that the central, compact, high-pressure component, which Laing & Bridle (2002b) argue is required to give the radio jet its observed structure, is transient on time-scales comparable to the lifetime of a radio source (and also to its own sound-crossing time). Generalizing the model of Laing & Bridle to other twin-jet sources, we might expect that their host galaxies would also contain dense central gas with a short cooling time. The *causal* nature of the relationship between the presence of this gas component and the the existence of a well-collimated jet is not clear – for example, we do not know whether there is a class of elliptical galaxies without a central hot-gas component in which jets form but are not recollimated and so do not give rise to strong radio emission. It is also not clear whether (or by what mechanism) the radio source can inject energy into the cooling gas and so maintain the high pressure gradient required for recollimation, though we note that the bolometric X-ray luminosity of the component represented by the smaller β model is a small fraction ($\sim 10^{-3}$) of the jet energy flux estimated by Laing & Bridle (2002b), so that the jet has energy to spare for such a mechanism. High-quality observations of more FRI radio sources, as well as of radio-quiet ellipticals, are required to answer these questions.

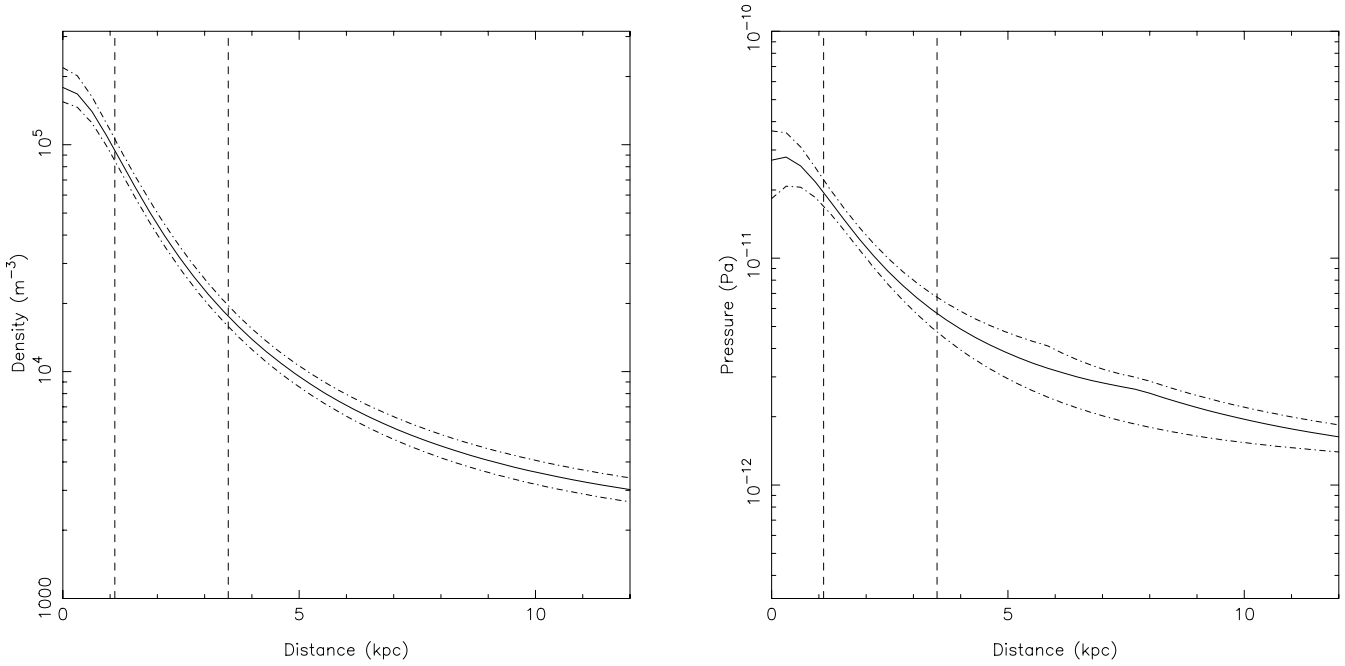

Figure 9. Proton density (left) and pressure (right) as a function of radius in 3C 31, based on the model described in the text. The solid black lines show the density and pressure derived from the best-fitting β models and the best-fitting straight line fit to the temperature data of Table 2. The surrounding dotted lines show the combined 1σ uncertainties due to the conversion between central normalization and density, the uncertainties on the β model fits and (in the case of pressure) the uncertainties on the linear fit to the temperature gradient. The slight discontinuity in the pressure gradient at $r \approx 8$ kpc arises because of the discontinuity in the simple temperature model we use. Because of the possible additional thermal component discussed in Section 7, the density and pressure may be underestimated in the inner 0.5 kpc. The vertical dotted lines show the boundaries of the jet regions defined by Laing & Bridle (2002a); the inner region (0 to 1.1 kpc), the flaring region (1.1 to 3.5 kpc) and the outer region (3.5 to 12 kpc).

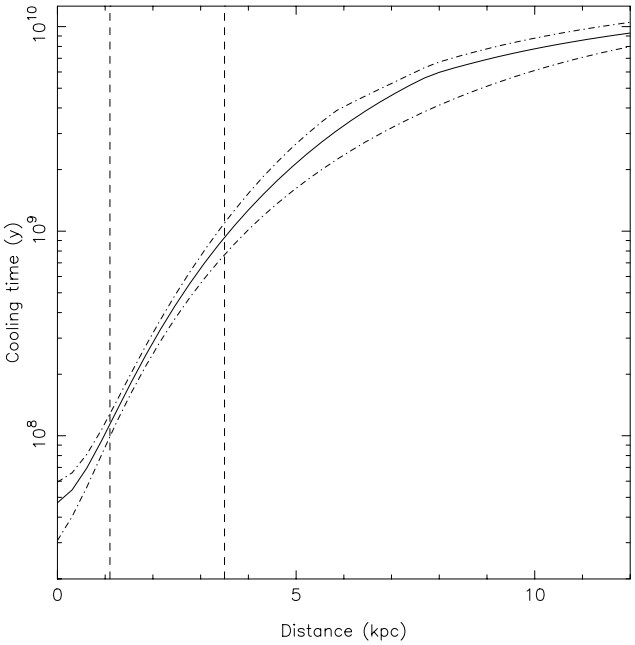

Figure 10. Cooling time as a function of radius in 3C 31. Lines and models as in Fig. 9.

8 CONCLUSION

We have used *Chandra* to observe the X-ray emission from the nucleus and the jet of 3C 31, and from hot gas in the inner regions of its group environment, as well as making X-ray detections of the other galaxies in the Arp 331 chain and of the nearby source 1E 0104+3153.

The non-thermal component of the X-ray core of 3C 31 is well modelled as a weakly absorbed power law, with no evidence for a more heavily absorbed hard component. We have argued that this implies that the X-ray emission originates outside any nuclear absorbing material. The power-law spectrum of 3C 31's core is relatively flat, and may be consistent with an inverse-Compton origin for the X-ray emission.

The X-ray flux density and spectrum of the jet of 3C 31 are well constrained. Because of its steep spectrum and because (in spite of uncertainties in the optical flux density) we can construct models which connect the radio and optical data smoothly to the X-ray, we attribute the X-ray emission from the jet to the synchrotron process. We know of no FRI radio source with a bright radio jet which does *not* have an X-ray jet, plausibly of synchrotron origin, when imaged deeply in the X-ray. It may be that the required high-energy, *in situ* particle acceleration is universal in these objects. The inner part of 3C 31's jet has a higher ratio of X-ray to radio emission than the rest of the jet. This is seen in a number of other sources (e.g., 3C 66B, Hardcastle et al. 2001; Cen A, Kraft et al. 2002) and may indicate a difference in the particle acceleration mechanism in this region.

Our observations have resolved for the first time the regions of 3C 31's hot-gas atmosphere where the radio jets are known to flare and decelerate (Laing & Bridle 2002a). There is significant evidence for a temperature gradient as well as a strong emissivity gradient as a function of radius. We have determined the density and pressure in this region as a function of radius, and have shown that the cooling time of this central hot-gas component is short. A

companion paper (Laing & Bridle 2002b) discusses the use of the density and temperature profiles to constrain the physical parameters of the jets.

Our luminosity measurements for the other galaxies of the Arp 331 chain are consistent with those of other workers, and in most cases the observed luminosities and spectra are best explained as originating in small-scale thermal emission associated with the galaxy. In the background source 1E 0104+3153, whose origin has long been uncertain, we infer, from the spatial and spectral properties of the X-ray source, that almost all the soft X-ray emission originates in the $z = 0.11$ group rather than the known BAL quasar close to the X-ray centroid. The quasar may contribute to the observed hard X-rays given a plausible intrinsic absorbing column.

ACKNOWLEDGMENTS

We are grateful to Judith Croston for providing optical flux densities for the 3C 31 jet region in advance of publication.

The National Radio Astronomy Observatory is a facility of the National Science Foundation operated under cooperative agreement by Associated Universities, Inc.

REFERENCES

Bicknell G.V., 1984, ApJ, 286, 68
Bicknell G.V., 1994, ApJ, 422, 542
Birkinshaw M., Worrall D.M., 1993, ApJ, 412, 568
Bowman M., Leahy J.P., Komissarov S.S., 1996, MNRAS, 279, 899
Burch S.F., 1977, MNRAS, 181, 599
Butcher H.R., van Breugel W., Miley G.K., 1980, ApJ, 235, 749
Canosa C.M., Worrall D.M., Hardcastle M.J., Birkinshaw M., 1999, MNRAS, 310, 30
Chiaberge M., Capetti A., Celotti A., 1999, A&A, 349, 77
Fabbiano G., Miller L., Trinchieri G., Longair M., Elvis M., 1984, ApJ, 277, 115
Fanaroff B.L., Riley J.M., 1974, MNRAS, 167, 31P
Fomalont E.B., Bridle A.H., Willis A.G., Perley R.A., 1980, ApJ, 237, 418
Forman W., Jones C., Tucker W., 1985, ApJ, 293, 102
Fraix-Burnet D., Golombek D., Macchetto F.D., Nieto J.-.L., 1991, AJ, 102, 562
Green P.J., Schartel N., Anderson S.F., Hewett P.C., Foltz C.B., Brinkmann W., Fink H., Truemper J., Margon B., 1995, ApJ, 450, 51
Hardcastle M.J., 2000, A&A, 357, 884
Hardcastle M.J., Alexander P., Pooley G.G., Riley J.M., 1997, MNRAS, 288, L1
Hardcastle M.J., Birkinshaw M., Worrall D.M., 2001, MNRAS, 326, 1499
Hardcastle M.J., Worrall D.M., 1999, MNRAS, 309, 969
Hardcastle M.J., Worrall D.M., 2000, MNRAS, 314, 359
Harris D.E., Biretta J.A.J., Junor W., 1997, MNRAS, 284, L21
Keel W.C., 1988, ApJ, 329, 532
Komossa S., Böhringer H., 1999, A&A, 344, 755
Kraft R.P., Forman W.R., Jones C., Murray S.S., Hardcastle M.J., Worrall D.M., 2002, ApJ in press (astro-ph/0111340)
Laing R.A., Bridle A.H., 2002a, MNRAS submitted
Laing R.A., Bridle A.H., 2002b, MNRAS submitted
Laing R.A., Parma P., de Ruiter H.R., Fanti R., 1999, MNRAS, 306, 513
Morganti R., Parma P., Capetti A., Fanti R., de Ruiter H.R., 1997, A&A, 326, 919
Perlman E.S., Sparks W.B., Radomski J., Packham C., Fisher R.S., Piña R., Biretta J.A., 2001, ApJ, 561, L51
Stocke J.T., Liebert J., Schild R., Gioia I.M., Maccacaro T., 1984, ApJ, 277, 43
Tansley D., Birkinshaw M., Worrall D.M., 2001, MNRAS submitted
Tavecchio F., Maraschi L., Sambruna R.M., Urry C.M., 2000, ApJ, 544, L23
Trussoni E., Massaglia S., Ferrari R., Fanti R., Feretti L., Parma P., Brinkmann W., 1997, A&A, 327, 27
Turner T.J., George I.M., Mushotzky R.F., Nandra K., 1997, ApJ, 475, 118
Ueno S., Koyama K., Nishida M., Yamauchi S., Ward M.J., 1994, ApJ, 431, L1
Whysong D., Antonucci R., 2001, ApJ submitted (astro-ph/0106381)
Wilson A.S., Yang Y., 2002, ApJ, 568, in press (astro-ph/0112097)
Worrall D.M., Birkinshaw M., 2000, ApJ, 530, 719
Worrall D.M., Birkinshaw M., Hardcastle M.J., 2001, MNRAS, 326, L7